Grain-Size-Dependent Diamond−Nondiamond Composite Films: Characterization and Field-Emission Properties

Debabrata Pradhan*,[†] and I. Nan Lin

Department of Physics, Tamkang University, Tamsui, Taipei, Taiwan, Republic of China

ABSTRACT Diamond films with grain sizes in the range of 5−1000 nm and grain boundaries containing nondiamond carbon are deposited on a silicon substrate by varying the deposition parameters. The overall morphologies of the as-deposited diamond−nondiamond composite films are examined by scanning electron microscopy and atomic force microscopy, which show a decrease in the surface roughness with a decrease in the diamond grain size. Although the Raman spectra show predominately nondiamond carbon features in the diamond films with smaller grain sizes, glancing-angle X-ray diffraction spectra show the absence of graphitic carbon features and the presence of very small amorphous carbon diffraction features. The CH_4 percentage (%) in Ar and H_2 plasma during deposition plays a crucial role in the formation of diamond films with different grain sizes and nondiamond carbon contents, which, in turn, determines the field-emission behavior of the corresponding diamond films. The smaller the grain size of the diamond, the lower is the turn-on field for electron emission. A lower turn-on field is obtained from the diamond films deposited with 2−5% CH_4 than from the films deposited with either 1% or 7.5% CH_4 in the Ar medium. A current density greater than 1 mA/cm^2 (at 50 V/μm) is obtained from diamond films deposited with a higher percentage of CH_4. A model is suggested for the field-emission mechanism from the diamond−nondiamond composite films with different diamond grain sizes and nondiamond contents.

KEYWORDS: field emission • nanodiamond • composites • plasma deposition

1. INTRODUCTION

Being a wide-band-gap semiconductor ($E_g = 5.5$ eV) along with having high resistivity, diamond thin films do not appear to be a suitable material for the electron field-emission (FE) applications. In the case of an undoped diamond, the concentration of electrons in the conduction band is almost too negligible to be emitted. In spite of the above-mentioned disadvantages, diamond has a series of excellent physical and chemical properties, which make it one of the strongly contending cold cathode materials for FE applications. Diamond has the most strongly bonded crystal structure, such that FE devices from diamond could operate with maximum stability and reliability. Furthermore, diamond can operate at high temperature or high power because of its very high electrical breakdown field and high thermal conductivity, properties highly beneficial to FE. Diamond also possesses a very small barrier potential at its surface for the electrons to leave and emit into vacuum because of a low work function (3.5 eV). When the diamond surface is terminated with H atoms, it shows a negative electron affinity (NEA) (1, 2) and is the only known material that is stable in air with NEA. With these attractive features of the diamond surface, adding the new ability to deposit diamond thin film on a variety of substrates using various low-pressure chemical vapor deposition (CVD) techniques has created vivid interest in the applications of diamond as an electron field emitter since the early 1980s. In 1991, low threshold field (∼3 V/μm) emission from diamond-based cathodes was reported by Wang et al. and Geis et al. (3, 4). Since then, extensive studies have been done on the FE properties of diamond or diamondlike carbon materials (5).

In the decade of the 1990s, most of the electron emission studies were carried out on a microcrystalline diamond (MCD) film, where the diamond grain sizes varied from 0.1 μm to several micrometers. These diamond films were usually deposited on a conducting silicon (Si) surface using H_2 plasma with a very low CH_4 concentration (∼1%). Eventually, it was found that the grain size of the diamond in the films could be varied with the deposition parameters. Nanocrystalline diamond (NCD) films of grain sizes in the range of 10−100 nm have been deposited using higher percentages of CH_4 in H_2 and with or without nitrogen (6−9). Furthermore, in the presence of H_2-deficient plasma (i.e., in CH_4/Ar, C_{60}/Ar, and CH_4/N_2 plasma), ultra-NCD (UNCD) films with grain sizes of less than 10 nm have been routinely obtained (10−13). With this drastic reduction of the diamond grain sizes in the presence of Ar-rich plasma, defects and conducting grain boundaries of the UNCD film surge to a pinnacle that promises far better FE properties. Although FE properties from these diamond films (MCD, NCD, and UNCD) are studied separately in detail (9, 12, 14), there are only a limited number of studies that compare their proper-

Table 1. Deposition Parameters to Obtain Different Types of Diamond Films

sample	deposition medium (%)	MW power (kW)	pressure (Torr)	time (h)	grain size (nm)
MCD	CH_4/H_2 (1:99)	1.8	50	3	1000
NCD	CH_4/H_2 (2:98)	1.8	50	3	20–30
UNCD-1	CH_4/Ar (1:99)	1.2	150	3	<10
UNCD-2	CH_4/Ar (2:98)	1.2	150	3	<10
UNCD-3	CH_4/Ar (3:97)	1.2	150	2	10–20
UNCD-5	CH_4/Ar (5:95)	1.2	150	2	20–25
UNCD-7.5	CH_4/Ar (7.5:92.5)	1.2	150	0.5	20–25

ties in detail. The FE properties from a polycrystalline CVD diamond vary inversely to the grain size (15) and differ from those of the NCD and UNCD films. In the present work, we have made an effort to understand the effect of a growth medium on the various properties of diamond films, in particular the competition between the diamond grain sizes and nondiamond contents, such as graphitic or amorphous carbon in the MCD, NCD, and UNCD films, for lowering the turn-on field and increasing the current density during the electron FE.

2. EXPERIMENTAL DETAILS

One-side-polished Si single-crystal wafers (p-type, boron-doped) from Wacker Chemitronic GmbH, having a (100) crystallographic orientation, were used as substrates for diamond film deposition. Si substrates were first thoroughly degreased by sonication in acetone and isopropyl alcohol, each for 5–10 min. Then they were subjected to 2 min of etching in a 40% HF solution for removal of the native oxide layer. Subsequently, Si substrates were sonicated in a diamond powder (30 nm size) and methanol slurry for 1 h. Then the substrates were rinsed thoroughly in methanol and again ultrasonicated for another 5 min in fresh methanol to remove any loosely bound diamond particles from Si surface. The pretreated Si substrates were finally dried under a nitrogen stream prior to loading into the deposition chamber. An IPLAS microwave plasma-enhanced CVD (MPECVD) system was used for diamond film deposition. The deposition parameters were varied to grow diamond films with different grain sizes and nondiamond contents. Table 1 presents detailed deposition conditions for MCD, NCD, and UNCD films. The total gas flow rate for all of the depositions was kept constant at 200 sccm (standard cubic centimeter per minute). No external heater was used to heat the substrate during deposition. The substrate temperature was measured to be 700–800 °C for the films deposited in the H_2 plasma, whereas it was 450–500 °C in the Ar plasma. All of the characterizations of the diamond films were carried out ex situ. The surface morphologies of the diamond films were examined with a JEOL FE scanning electron microscope. Atomic force microscopic (AFM) analyses were carried out under ambient conditions with a scanning probe microscope (Digital Instruments Nanoscope IV) in noncontact mode using a Si tip (tip radius 5–10 nm). Raman spectra of the samples were recorded with a Renishaw spectrometer in a back-scattering geometry. A 514.0 nm Ar laser line was used for exciting the diamond films to collect the Raman signals. Glancing-angle X-ray diffraction (GIXRD) patterns of the samples were collected with a PANalytical X-ray diffractometer using a Cu Kα line (1.54 Å) from an X-ray generator operated at 40 kV and 40 mA. The FE measurements were performed at a low pressure of 10^{-6} Torr. The voltage to the cathode was applied by an analog programmable power supply (Keithley 237) under computer control, and the measured emission current was logged at each voltage.

3. RESULTS AND DISCUSSION

3.1. Morphologies and Topologies of Diamond Films.
Parts (a,b), (c,d) and (e,f) of Figure 1 show the surface morphologies of MCD, NCD, and UNCD-1 films, respectively, with their deposition conditions presented in Table 1. The UNCD films deposited at a higher CH_4 concentration (2–7.5%) in an Ar medium show morphologies [scanning electron microscopy (SEM) images not shown] almost similar to those of the UNCD-1 film except the formation of elongated clusters of diamond grains for UNCD-5 and UNCD-7.5 films and a slight increase in the grain size (see Table 1). The overall surface morphology evidently shows a decrease in the surface roughness with a decrease in the grain size of the diamond crystal. At 1% CH_4 in H_2, diamond grains of size ~1.0 μm are formed (Figure 1a,b). The diamond crystals in the MCD film appear to be well faceted (Figure 1b). With an increase in the CH_4 percentage to 2% in the same H_2 medium, the diamond grain size is reduced to 20–30 nm, forming a NCD film (Figure 1c,d). The decrease in the grain size at 2% CH_4 in H_2 is due to the secondary nucleation, which is known to occur during the diamond deposition with a higher percentage of CH_4 (16, 17). The mechanism of MCD formation involving CH_3 and a H^+ radical formed by H_2 gas plasma is well established (18). For the deposition of films with much finer diamond crystals of size <10 nm, Ar is usually used as the major gas. Parts e and f of Figure 1 show the surface morphology of a UNCD film obtained in the plasma of 1% CH_4 (2 sccm) and 99% Ar (198 sccm). The C_2 radical was originally suggested to be the main component for the formation of finer diamond crystals in a NCD/UNCD film deposited in an Ar medium (11, 19). In recent reports, May et al. and others found that C_2 radical species do not play a major role in the formation of NCD and UNCD films in Ar/H_2/CH_4 and He/H_2/CH_4 media (20–23). They propose that most of the diamond is formed via a mechanism similar to that of MCD films, i.e., gas-phase H atoms abstracting surface H atoms, followed by CH_x, $x = 0$–3, addition. From the theoretical and experimental evidence, they also suggested that the CH_3 and C atoms are the most likely precursors for the growth of UNCD (21). The decrease in the diamond grain size from the MCD film to the UNCD film simultaneously increases the grain boundary area, which is believed to be filled with nondiamond or graphitic carbon, thereby enhancing the electrical conductivity of the films. Better electron conduction in the film facilitates higher FE from the UNCD and NCD films as compared to that of the MCD film (discussed later).

Parts a–c of Figure 2 show the AFM images of MCD, NCD, and UNCD-1 films, respectively. While the crystal facets are evident from the MCD film, the AFM images from the NCD and UNCD-1 films display cauliflower-like growth. The surface topologies of the aforementioned diamond films are well matched to the SEM images (Figure 1). Table 2 summarizes the root-mean-square (rms) surface roughness of individual films at different scan ranges. The smaller surface roughness from the NCD and UNCD films as compared to
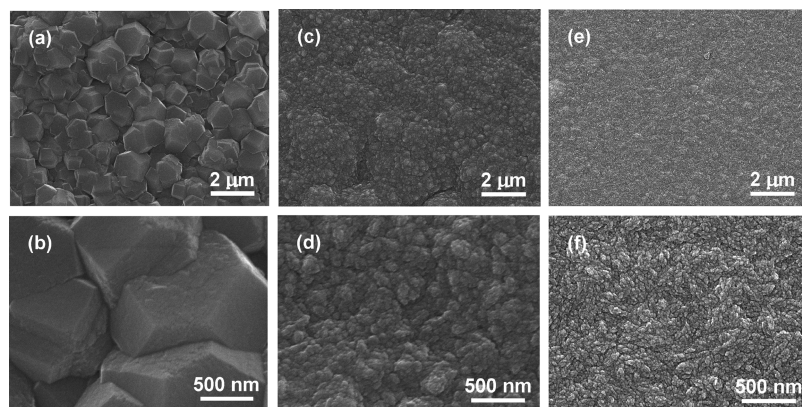
FIGURE 1. SEM images of (a and b) MCD, (c and d) NCD, and (e and f) UNCD-1 films.
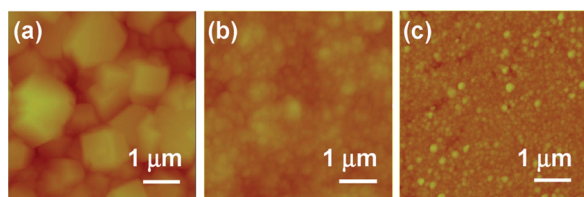

FIGURE 2. AFM images of (a) MCD, (b) NCD, and (c) UNCD-1 films.

Table 2. Root-Mean-Square Surface Roughness (nm) for MCD, NCD, and UNCD-1 Films at Different Scan Ranges

scan range	MCD	NCD	UNCD-1
$5 \mu m \times 5 \mu m$	152.35	67.47	13.70
$3 \mu m \times 3 \mu m$	116.05	56.47	13.23
$1 \mu m \times 1 \mu m$	91.33	30.85	11.27

that of the MCD film is apparently due to the decrease in the diamond grain size and a higher diamond nucleation density. The smallest surface roughness obtained from the UNCD film makes it a highly desirable material for surface acoustic devices, microelectromechanical systems, and other tribological applications (24−27).

3.2. Structural Properties of Diamond Films.
Parts a−c of Figure 3 show the Raman spectra of MCD, NCD, and UNCD-1 films, respectively. The broad Raman features obtained from both the NCD and UNCD-1 films are deconvoluted to identify individual peak positions. The first-order
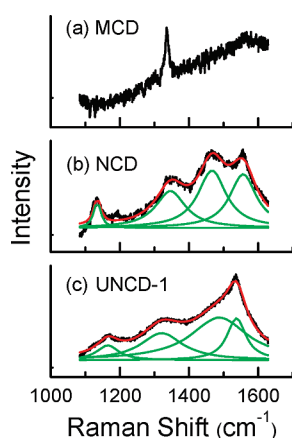

FIGURE 3. Raman spectra of (a) MCD, (b) NCD, and (c) UNCD-1 films.

zone center sharp Raman peak of diamond and graphite is lies at 1332.5 ± 0.5 and 1580 ± 0.5 cm^{-1}, respectively. All other types of carbon show broad features between 1100 and 1600 cm^{-1} (28, 29). A singular intense peak obtained from the MCD film, as shown in Figure 3a, confirms the diamond phase. Moreover, the broadness of the peak [with a full width at half-maximum (fwhm) of 8.34 cm^{-1}] and positioning at a higher wavenumber (1335.0 cm^{-1}) than its original position (1332.5 cm^{-1}), with an additional shoulder at around 1560 cm^{-1}, clearly suggest the presence of defects and nondiamond contents in the MCD film. The Raman spectrum obtained from the NCD film (Figure 3b) is completely different from that of the MCD film with the absence of a sharp first-order diamond peak at ∼1332.0 cm^{-1}. The broad Raman features obtained from NCD and UNCD-1 films show four major bands, and those bands are well matched to the literature (10, 30). The Raman bands observed at ∼1350 and 1550 cm^{-1} are normally termed as the D band (disorder/defect band) and G band (graphitic/E_{2g2} band), respectively. Two additional features in the Raman spectra of NCD and UNCD films are located at 1150−1180 and 1470 cm^{-1}, occasionally used as fingerprints of UNCD films. These bands are now known to be due to the vibrations of sp^2 chains in the polyacetylene segments present at the grain boundaries and at the surface of NCD and UNCD films (31, 32). It must be noted that the absence of a sharp feature at ∼1332 cm^{-1} in the NCD and UNCD films is due to the use of visible Raman spectroscopy, which is more sensitive toward sp^2-bonded carbon. Therefore, although NCD and UNCD films are primarily constituted of diamond grains, the Raman feature of diamond at ∼1332.0 cm^{-1} is almost invisible. The Raman spectra of UNCD films deposited with a higher percentage of CH$_4$ are almost similar to that of UNCD-1 with the exception of increases in the 1350 and 1470 cm^{-1} peak intensities with an increase in the percentage of CH$_4$, which suggests an increase in the disorder carbon and transpolyacetylene segments of carbon.

Parts a−c of Figure 4 show the GIXRD spectra from MCD, NCD, and UNCD-1 films, respectively. The presence of diffraction features at 2θ values (crystal plane) of 43.95° (111), 75.75° (220), and 91.85° (311) is in good accord with a cubic diamond (JCPDS reference file 00-011-1249). The increase in the fwhm of the prominent (111) diffraction
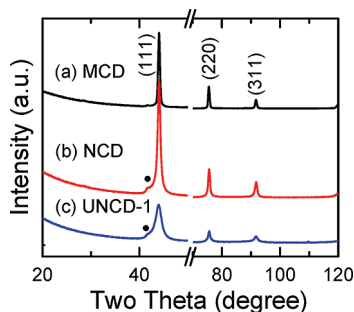
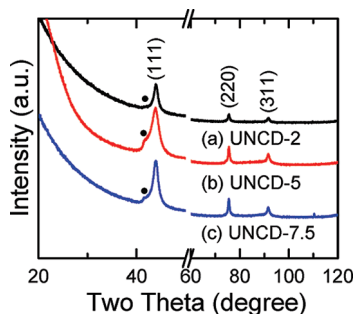FIGURE 4. GIXRD spectra of (a) MCD, (b) NCD, and (c) UNCD-1 films.

FIGURE 5. GIXRD spectra of (a) UNCD-2, (b) UNCD-5, and (c) UNCD-7.5 films.

feature from MCD to NCD to UNCD films can be correlated to their decrease in the crystalline grain size and thereby the increase in grain boundaries containing nondiamond contents. Although both the NCD and UNCD films possess large areas of grain boundaries, no diffraction peak is obtained at 2θ of 26.3° for the 002 crystal plane of graphite. This apparently suggests that both NCD and UNCD films are primarily constituted of diamond grains and the amount of graphitic carbon inside these films cannot be detected by GIXRD. A smaller feature at 2θ of 41.85° (marked by a solid dot) is present only in the case of NCD and UNCD films, which is possibly due to a small quantity of amorphous carbon. While Raman spectra primarily show the presence of the nondiamond phase, GIXRD evidently gives diffraction features from the diamond crystal. The results from both the Raman and GIXRD qualitatively agree with the higher diamond contents in the MCD film and higher nondiamond contents in the UNCD-1 film.

Figure 5 shows GIXRD spectra of UNCD films obtained at higher CH_4 concentration (2%, 5%, and 7.5%). It was previously known that, with an increase in the percentage of CH_4 in a H_2 medium, diamond film coverts to a nanocrystalline graphite film (33). Unlike the case of diamond film growth in a H_2 medium at a higher percentage of CH_4, UNCD films obtained with 2−7.5% CH_4 in an Ar medium do not show a significant increase in the nondiamond content. No XRD feature from graphite is obtained in the 2θ range of 23−26°, and the feature at 41.85° for amorphous carbon is slightly increased with an increase in the percentage of CH_4. This suggests that the rate of formation of nondiamond carbon in the Ar medium is significantly slower and the UNCD films deposited even at 7.5% CH_4 possess primarily diamond character. This could be a reason for the best FE
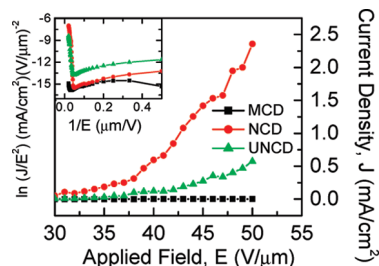

FIGURE 6. $J-E$ plots from (a) MCD, (b) NCD, and (c) UNCD-1 films. The inset shows the corresponding F−N plots.

Table 3. Turn-on Field and Current Density (at 50 V/μm) Measured from the Diamond Films Deposited at Different Conditions

sample	deposition medium (%)	turn-on field (V/μm)	current density (mA/cm^2)
MCD	CH_4/H_2 (1:99)	30	0.85×10^{-3}
NCD	CH_4/H_2 (2:98)	13	2.35
UNCD-1	CH_4/Ar (1:99)	14.7	0.57
UNCD-2	CH_4/Ar (2:98)	8.69	0.35
UNCD-3	CH_4/Ar (3:97)	9.34	0.25
UNCD-5	CH_4/Ar (5:95)	9.0	1.99
UNCD-7.5	CH_4/Ar (7.5:92.5)	13.99	3.09

from NCD films deposited with 2 sccm of CH_4 in a H_2 medium (9, 34, 35), unlike the present work, which finds 2−5% CH_4 (4−10 sccm of CH_4) in an Ar medium during diamond deposition showing the best FE properties (discussed later).

3.3. FE Properties of Diamond Films. Figure 6 shows the representative plots of current density J (mA/cm^2) as a function of the applied electric field E (V/μm) for MCD, NCD, and UNCD films, and the inset shows corresponding Fowler−Nordheim (F−N) plots. The turn-on electric field was measured by extrapolating two straight lines on both the lower and higher sides of the electric field in the F−N plot (36). Table 3 displays the emission properties from the diamond films deposited under the conditions listed in Table 1. To explain the emission behavior from different types of diamond films, a schematic model diagram is presented in Figure 7. The gray and white regions in Figure 7a−c are represented as nondiamond contents and diamond grains, respectively. The turn-on field from the MCD film (30 V/μm) is the highest among the diamond films. The MCD film was deposited in a complete H_2 medium, making the surface partially hydrogenated, which could reduce the electron affinity and promote emission at a lower applied field. The smaller work function of diamond (3.5 eV) as compared to graphite (5.0 eV), as shown in the band diagram (Figure 7d,e), is another reason for easy electron emission from the MCD film. Furthermore, the larger grain size of the MCD film has a favored geometry to give a higher field enhancement factor, which is advantageous to electron emission. Despite all of these favorable properties, a higher turn-on field from the MCD film in comparison to UNCD films (deposited in a H_2-free atmosphere) suggests that a smaller quantity of nondiamond contents because of larger grain sizes of diamond is not suited to obtain higher FE properties. The larger
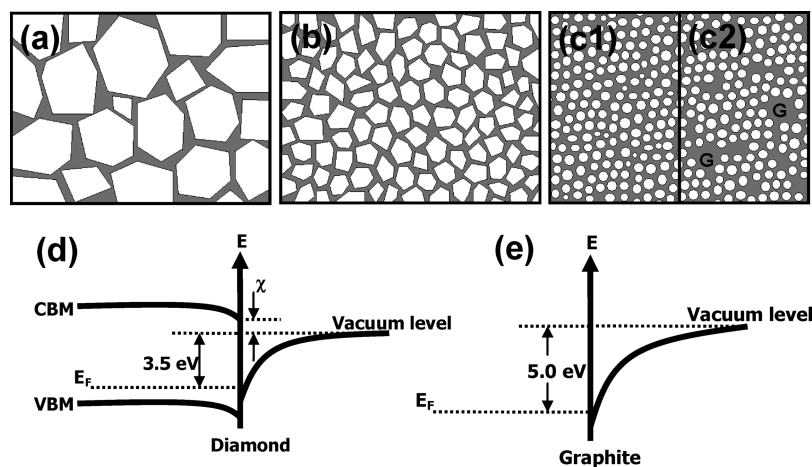
ACS **APPLIED** MATERIALS &INTERFACES

FIGURE 7. Schematic model diagram of (a) MCD, (b) NCD, and UNCD films with (c1) smaller and (c2) larger quantities of nondiamond contents. The white and gray regions represent diamond and nondiamond contents (amorphous and/or graphitic carbon), respectively. Band diagrams of single-crystal (d) diamond and (e) graphite. The nondiamond carbon contents in the film are extremely essential for the easy electron conduction inside the matrix and also from back to front surface of the film before being emitted from the edges of the diamond grain experiencing a lower work function of 3.5 eV.

size diamond grain reduces the electron conduction in the MCD film and therefore requires a higher electric field for emission to occur. When deposition is performed at 2 % CH_4 in a H_2 medium, which produces the NCD film, it shows FE at a relatively lower turn-on field (13 V/μm). This is obviously due to the higher concentration of CH_4 used in the deposition of the NCD film, which not only reduces the diamond grain size to 20−30 nm (Figure 1c,d) but also increases the nondiamond contents inside the film, as confirmed from the Raman spectrum (Figure 3b). This indicates that the grain sizes and nondiamond contents in the diamond films are prime requirements for FE to occur at a lower turn-on field. Interestingly, a further decrease in the grain size to <10 nm in the case of the UNCD-1 film did not show a lower turn-on field as compared to the NCD film of grain size 20−30 nm. The lower turn-on applied field from the NCD film (13 V/um, deposited with 2 % CH_4 in H_2) in comparison to that of the UNCD-1 film (14.7 V/um, deposited with 1 % CH_4 in an Ar medium) implies that higher nondiamond contents, formed as a result of a higher percentage of CH_4 used in the deposition, have a stronger effect than the grain size when varied from 20−30 to 10 nm. However, the turn-on fields from the NCD and UNCD-1 films are fairly close and therefore exact ratiocination is difficult.

Among the UNCD films, lower turn-on fields of 8−9 V/μm are obtained from the UNCD films deposited with 2−5 % CH_4. The UNCD films deposited either at lowest (1 %) or at highest (7.5 %) CH_4 in an Ar medium show higher turn-on fields. The present result is different from previous report (9), which shows a decrease in the FE behavior (an increase in the turn-on field) of the NCD film deposited in a N_2 medium with an increase in CH_4 flow from 1.4 to 5.6 % CH_4 (2.1−8.4 sccm of CH_4). This could be due to the significant increase in nondiamond contents in the film that degrades the FE properties. Nitrogen is known to preferentially incorporate in the grain boundary region because of a lower substitutional energy and easier bond distortion in the grain boundary region (37). The nitrogen incorporation increases the sp^2-bonded carbon, leading to broadening of π and π^*

states, making the film more metallic with an increase in the nitrogen content, as confirmed from the conductivity measurements (38). However, in the present work, the turn-on field remains lower with the deposition at 2−5 % CH_4 (4−10 sccm of CH_4), indicating a smaller increase in the nondiamond contents, which is in accordance with the GIXRD results (Figure 5). However, the turn-on field is found to increase to 13.99 V/μm for the UNCD-7.5 film (deposited with 7.5 % CH_4, i.e., 15 sccm), suggesting an increase in the nondiamond contents above an optimum value for the best FE. Although nondiamond contents enhance the electrical conductivity (38) and therefore allow emission to occur at a lower applied field, it has a high work function (the work function of graphite is 5.0 eV) than that of the diamond (3.0 eV). The nondiamond carbon content can be increased in the diamond film either by nitrogen incorporation or by use of higher CH_4 during deposition. The increase of the conductivity by nitrogen incorporation is studied in detail (38, 39). Therefore, in a composite film, which is constituted from both the diamond and nondiamond carbon, there is a competition in between the diamond and nondiamond properties for higher FE properties. Cui et al. have proposed a model describing that emission only occurs from the edges of the diamond grains, where electrons experience a lower work function of diamond (3.5 eV), whereas no emission is contributed from nondiamond or graphitic carbon (40). This can be seen in the schematic model diagram (Figure 7a−c), where there is an increase in the grain boundary area with a decrease in the grain size. However, when nondiamond contents become extremely high (marked as G in the gray region of Figure 7c2), emission from those parts needs a higher applied field because of the high work function of graphite, i.e., 5.0 eV. Hence, the UNCD film deposited at 7.5 % CH_4 shows a slightly higher turn-on field as compared to films deposited with 2−5 % CH_4. The present study therefore demonstrates that UNCD films deposited in a wider CH_4 concentration (2−5 %) range can be used to obtained higher FE properties as compared to <2 % CH_4 for NCD films grown in a N_2 medium (9). It also indicates that
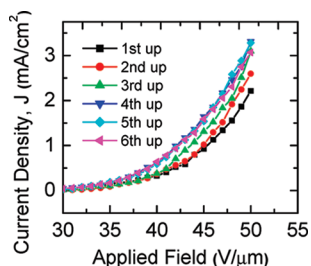
FIGURE 8. *J–E* plot obtained from the UNCD-7.5 film by repeated measurement at the same location.

the rates of formation of nondiamond contents in Ar and N_2 media are different and therefore the optimum percentages of CH_4 needed for higher FE properties are found to be different for UNCD, NCD, and MCD films (9). Furthermore, we have measured the current density (at 50 V/μm) from all of the diamond films. The current densities are found to be greater than 1 mA/cm^2 for the NCD, UNCD-5, and UNCD-7.5 films, indicating that a higher percentage of CH_4 during deposition leads to more nondiamond contents in the films and therefore easy electron conduction and higher emission (41). From the values presented in Table 3, it can be concluded that an optimum ratio of diamond to nondiamond carbon contents (which depends on the flow rate of precursor gases) is needed to obtain lower turn-on fields (UNCD-2, UNCD-3, and UNCD-5 films), whereas higher nondiamond contents are needed to obtain higher current densities (NCD, UNCD-5, and UNCD-7.5 films).

Instability in the FE could arise when nondiamond carbon contents increase above a certain level inside the diamond films. Wu et al. reported no observable emission from the NCD films deposited above 4.9 sccm of CH_4 (3.2 %) flow rate in a N_2 medium (9). Therefore, we performed repeated measurements at the same location of diamond films to study the stability and reproducibility of the emission behavior. Figure 8 shows the emission from the diamond film deposited at the highest CH_4 (7.5 %) used in the present work. A discernible improvement (a lowering in the turn-on field and an increase in the current density) in the emission is observed after three cycles of emissions, which is attributed to the surface cleaning. The overall reproducibility of the emission suggests that the diamond film depositing up to 7.5 % CH_4 (15 sccm) in the present work is stable.

4. CONCLUSIONS

Diamond thin films of different grain sizes are deposited on Si substrates using the MPECVD technique. The overall morphologies of the as-deposited films, as investigated by SEM and AFM, show a decrease in the surface roughness with a decrease in the grain size of the diamond (from MCD to NCD to UNCD films). Raman spectroscopic measurements carried out on different diamond films suggest higher nondiamond contents inside the NCD and UNCD films than inside the MCD film. However, the GIXRD spectra show no diffraction features of graphite and a very small diffraction feature of amorphous carbon (at 2θ of 41.85°), which suggests that all of the diamond films are primarily consti-

tuted of diamond grains. The results from both the Raman and GIXRD spectra clarify that diamond films are composites of diamond grains and nondiamond carbon in the grain boundaries. A lower turn-on field is obtained from UNCD films because of smaller diamond grains and a large area of grain boundaries. The nondiamond contents in the grain boundaries play a significant role in the electron transport for FE to occur at a lower applied field. The turn-on field is further reduced by depositing UNCD films at an optimum CH_4 concentration of 2−5 %. However, the increase in the turn-on field from the UNCD film deposited at 7.5 % CH_4 is due to exceedingly nondiamond contents, and therefore the electrons experience a higher work function of graphite for FE. On the other hand, the current density measured at an applied field of 50 V/μm is higher from the diamond films deposited with a higher percentage of CH_4. A reproducible emission is obtained from the same location of the UNCD film deposited with 7.5 % CH_4, which suggests the high emission stability from the UNCD films.

REFERENCES AND NOTES

(1) Pate, B. B. *Surf. Sci.* **1986**, *165*, 83.
(2) van der Weide, J.; Zhang, Z.; Baumann, P. K.; Wensell, M. G.; Bernholc, J.; Nemanich, R. J. *Phys. Rev. B* **1994**, *50*, 5803.
(3) Wang, C.; Garcia, A.; Ingram, D. C.; Lake, M.; Kordesch, M. E. *Electron. Lett.* **1991**, *27*, 1459.
(4) Geis, M. W.; Efremow, N. N.; Woodhouse, J. D.; McAleese, M. D.; Marchywka, M.; Socker, D. G.; Hochedez, J. F. *IEEE Electron Device Lett.* **1991**, *12*, 456.
(5) Xu, N. S.; Huq, S. E. *Mater. Sci. Eng. R* **2005**, *48*, 47.
(6) Catledge, S. A.; Vohra, Y. K. *J. Appl. Phys.* **1999**, *86*, 698.
(7) Yang, W. B.; Lu, F. X.; Cao, Z. X. *J. Appl. Phys.* **2002**, *91*, 10068.
(8) Jiang, N.; Kujime, S.; Ota, I.; Inaoka, T.; Shintani, Y.; Makita, H.; Hatta, A.; Hiraki, A. *J. Cryst. Growth* **2000**, *218*, 265.
(9) Wu, K.; Wang, E. G.; Cao, Z. X.; Wang, Z. L.; Jiang, X. *J. Appl. Phys.* **2000**, *88*, 2967.
(10) Xiao, X.; Birrell, J.; Gerbi, J. E.; Auciello, O.; Carlisle, J. A. *J. Appl. Phys.* **2004**, *96*, 2232.
(11) Gruen, D. M. *Annu. Rev. Mater. Sci.* **1999**, *29*, 211.
(12) Zhou, D.; Krauss, A. R.; Qin, L. C.; McCauley, T. G.; Gruen, D. M.; Corrigan, T. D.; Chang, R. P. H.; Gnaser, H. *J. Appl. Phys.* **1997**, *82*, 4546.
(13) Zhou, D.; McCauley, T. G.; Qin, L. C.; Krauss, A. R.; Gruen, D. M. *J. Appl. Phys.* **1998**, *83*, 540.
(14) Krauss, A. R.; Auciello, O.; Ding, M. Q.; Gruen, D. M.; Huang, Y.; Zhirnov, V. V.; Givargizov, E. I.; Breskin, A.; Chechen, R.; Shefer, E.; Konov, V.; Pimenov, S.; Karabutov, A.; Rakhimov, A.; Suetin, N. *J. Appl. Phys.* **2001**, *89*, 2958.
(15) Zhu, W.; Kochanski, G. P.; Jin, S.; Seibles, L. *J. Appl. Phys.* **1995**, *78*, 2707.
(16) Sharda, T.; Soga, T.; Jimbo, T.; Umeno, M. *Diam. Rel. Mater.* **2000**, *9*, 1331.
(17) Hong, S.-P.; Yoshikawa, H.; Wazumi, K.; Koga, Y. *Diamond Relat. Mater.* **2002**, *11*, 877.
(18) Harris, S. J. *Appl. Phys. Lett.* **1990**, *56*, 2298.
(19) Zhou, D.; McCauley, T. G.; Qin, L. C.; Krauss, A. R.; Gruen, D. M. *J. Appl. Phys.* **1998**, *83*, 540.
(20) May, P. W.; Ashfold, M. N. R.; Mankelevich, Y. A. *J. Appl. Phys.* **2007**, *101*, 053115.
(21) May, P. W.; Harvey, J. N.; Smith, J. A.; Mankelevich, Y. A. *J. Appl. Phys.* **2006**, *99*, 104907.
(22) May, P. W.; Mankelevich, Yu. A. *J. Appl. Phys.* **2006**, *100*, 024301.

(23) Rabeau, J. R.; John, P.; Wilson, J. I. B.; Fan, Y. *J. Appl. Phys.* **2004**, *96*, 6724.

(24) Assouar, M. B.; Elmazria, O.; Kirsch, P.; Alnot, P.; Mortet, V.; Tiusan, C. *J. Appl. Phys.* **2007**, *101*, 114507.

(25) Auciello, O.; Birrell, J.; Carlisle, J. A.; Gerbi, J. E.; Xiao, X.; Peng, B.; Espinosa, H. D. *J. Phys.: Condens. Matter* **2004**, *16*, R539.

(26) Srinivasan, S.; Hiller, J.; Kabius, B.; Auciello, O. *Appl. Phys. Lett.* **2007**, *90*, 134101.

(27) Sumant, A. V.; Grierson, D. S.; Gerbi, J. E.; Birrell, J.; Lanke, U. D.; Auciello, O.; Carlisle, J. A.; Carpick, R. W. *Adv. Mater.* **2005**, *17*, 1039.

(28) Robertson, J. *Adv. Phys.* **1986**, *35*, 317.

(29) Bachmann, P. K.; Wiechert, D. U. *Diamond and Diamond-Like Films and Coatings*; Clausing, R. E., Horton, L. L., Angus, J. C., Koidl, P., Eds.; NATO ASI Series 266; Plenum Press: New York, 1991; pp 677–713.

(30) Veres, M.; Tóth, S.; Koós, M. *Appl. Phys. Lett.* **2007**, *91*, 031913.

(31) Ferrari, A. C.; Robertson, J. *Phys. Rev. B* **2001**, *63*, 121405.

(32) Kuzmany, H.; Pfeiffer, R.; Salk, N.; Gunther, B. *Carbon* **2004**, *42*, 911.

(33) Li, X.; Perkins, J.; Collazo, R.; Nemanich, R. J.; Sitar, Z. *Diamond Relat. Mater.* **2006**, *15*, 1784.

(34) Okano, K.; Koizumi, S.; Silva, S. R. P.; Amaratunga, G. A. J. *Nature* **1996**, *381*, 140.

(35) Zhu, W.; Kochanski, G. P.; Jin, S. *Science* **1998**, *282*, 1471.

(36) Vander Ziel, A. *Solid State Physical Electronics*; Prentice-Hall: Englewood Cliffs, NJ, 1968.

(37) Zapol, P.; Sternberg, M.; Curtiss, L. A.; Frauenheim, T.; Gruen, D. M. *Phys. Rev. B* **2002**, *65*, 045403.

(38) Achatz, P.; Williams, O. A.; Bruno, P.; Gruen, D. M.; Garrido, J. A.; Stutzmann, M. *Phys. Rev. B* **2006**, *74*, 155429.

(39) Williams, O. A. *Semicond. Sci. Technol.* **2006**, *21*, R49.

(40) Cui, J. B.; Ristein, J.; Ley, L. *Phys. Rev. B* **1999**, *60*, 16135.

(41) Cui, J. B.; Stammler, M.; Ristein, J.; Ley, L. *J. Appl. Phys.* **2000**, *88*, 3667.